Geophysical Journal International

Geophys. J. Int. (2021) **227,** 54–57
Advance Access publication 2021 May 27
gjiras/700

https://doi.org/https://doi.org/10.1093/gji/ggab208

The hazard of coseismic gaps: the 2021 Fukushima earthquake

Eric Kiser and Haiyang Kehoe

Department of Geosciences, University of Arizona, 1040 *E 4th St, Tucson, AZ* 85721*, USA. E-mail: ekiser@arizona.edu*

Accepted 2021 May 25. Received 2021 May 24; in original form 2021 March 19

SUMMARY

Subduction zones are associated with significant seismic hazards around the world and determining the future locations of large earthquakes within these systems is a perpetual challenge of the Earth sciences. This study presents back-projection results from the 2021 M_w 7.1 Fukushima earthquake which show that the rupture area of this event filled a previously identified coseismic gap within the rupture area of the 2011 M_w 9.1 Tohoku-oki earthquake. These results, combined with observations of a similar coseismic gap from the 2010 M_w 8.8 Maule, Chile earthquake that was subsequently filled by a M_w 7.1 aftershock, demonstrate that future assessments of seismic hazards following giant earthquakes should include the identification of coseismic gaps left within main shock rupture areas.

Key words: Earthquake hazards; Earthquake interaction, forecasting, and prediction; Earthquake source observations.

Aftershock sequences, which are associated with stress changes from major earthquakes (e.g. King *et al.* 1994), pose significant seismic hazards around the world (e.g. Utsu 1970; Reasenberg & Jones 1989; Stein & Liu 2009). At subduction zones, portions of the plate interface adjacent to megathrust rupture areas are subjected to particularly large stress changes (e.g. Kaneko *et al.* 2010; Corbi *et al.* 2017) and tend to be regions where the largest aftershocks are located (e.g. Wetzler *et al.* 2018). This study shows that large and potentially devastating aftershocks also occur within the main shock slip area where rupture behaviour abruptly changes (e.g. gaps in the slip distribution) during megathrust events.

On 13 February 2021, the M_w 7.1 Fukushima earthquake occurred approximately 60 km offshore of Fukushima Prefecture, Japan at a depth of 55 km (Fig. 1a). This event was located near the downdip portion of the seismic plate interface, where the sources of high-frequency seismic radiation that produce strong ground shaking in coastal regions have been observed for several large earthquakes (e.g. Lay *et al.* 2012). Strong ground shaking from the 2021 Fukushima event was widespread, resulting in more than 180 injuries, one fatality and power outages at over 950 000 households within the Tohoku and Kanto regions. The earthquake also triggered landslides along the east coast of Honshu, Japan, leading to the disruption of coastal road networks in this region.

The 2021 Fukushima event occurred within the general rupture area of the 2011 M_w 9.1 Tohoku-oki megathrust earthquake, where one might expect a lower likelihood of large aftershock occurrence due to strain release during the 2011 main shock. Several studies that investigated the high-frequency rupture properties of the 2011 Tohoku-oki earthquake showed that the rupture jumped as much as 70 km distance as it propagated from northeast to southwest along the coast of Honshu (Fig. 1a; Movie S1; Wang & Mori 2011; Asano & Iwata 2012; Kiser & Ishii 2012; Yao *et al.* 2012). The seismic hazard potential of this 'coseismic gap' became apparent following a study of the 2010 M_w 8.8 Maule, Chile megathrust earthquake and aftershock sequence (Kiser & Ishii 2013). As in the Tohoku-oki case, the Maule, Chile megathrust earthquake exhibited a large gap in the downdip sources of high-frequency seismic waves during the rupture. Though the Maule, Chile megathrust earthquake produced a vigorous aftershock sequence in the months following the event, there was only one major earthquake ($M_w \geq 7$) that occurred near the plate interface within the megathrust rupture area. This M_w 7.1 aftershock occurred in 2012 and filled the coseismic gap associated with the 2010 main shock in the downdip portion of the plate interface (Fig. 1c). This observation indicated that coseismic gaps are regions where the plate interface does not fail during megathrust events and therefore are primed to be the locations of future large earthquakes. Based upon this interpretation, it was inferred that the Tohoku-oki coseismic gap also had the potential to produce a large event (Kiser & Ishii 2013).

Though it is evident that the epicentre of the 2021 Fukushima earthquake is within the 2011 Tohoku-oki coseismic gap (Fig. 1a), further analysis is needed to determine if the rupture area of this event caused failure throughout this portion of the subduction zone. To assess this possibility, we perform a back-projection analysis (Ishii *et al.* 2005) of the M_w 7.1 earthquake using seismic data from North America to constrain the event's rupture properties (Fig. S1). The back-projection method time shifts and stacks waveforms recorded at a seismic network to a grid of potential source locations to determine the spatiotemporal evolution of the earthquake rupture properties (Ishii *et al.* 2005; Kiser & Ishii 2017). In this study, bandpass filtered data (0.5–2 Hz) are back-projected to a 2° by 2° grid of potential source locations centred around the hypocentre of the 2021 M_w 7.1 Fukushima earthquake with a grid spacing of 0.05°. Traveltimes for the back-projection analysis are calculated

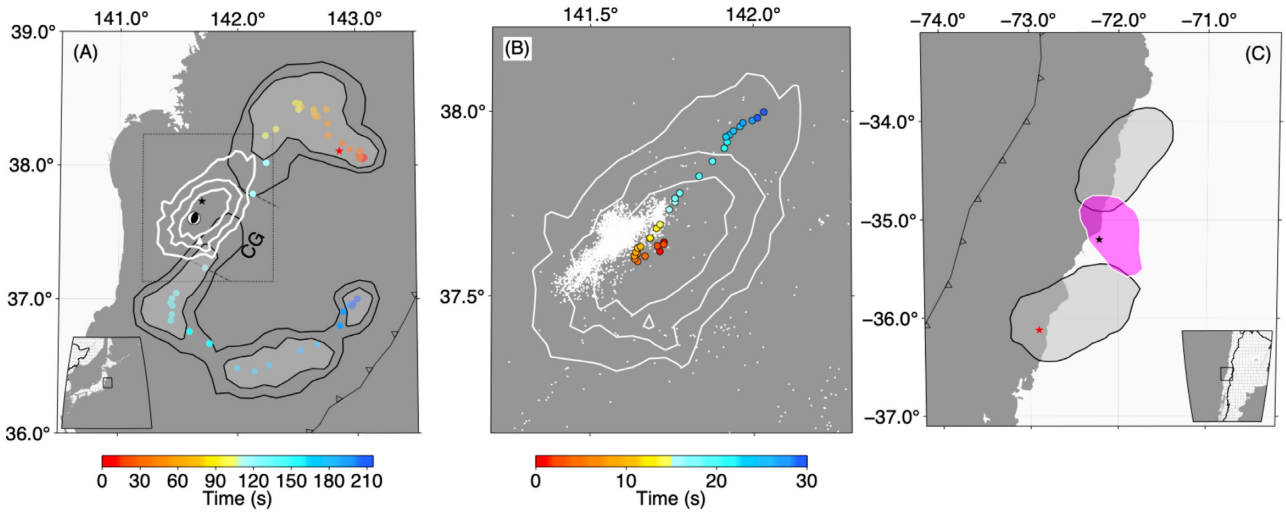

Figure 1. Rupture areas of the 2021 M_w 7.1 Fukushima and 2012 M_w 7.1 Chile earthquakes and their relationships to the Tohoku-oki, Japan and Maule, Chile coseismic gaps. (a) White contours show normalized integrated stack amplitudes from the back-projection analysis of the 2021 M_w 7.1 Fukushima earthquake. Contours greater than or equal to 0.7 are plotted using an interval of 0.1. The black star and beachball are the epicentre [Japan Meteorological Agency (JMA) catalogue] and focal mechanism (Global Centroid Moment Tensor catalogue; Ekström *et al*. 2012) of the Fukushima earthquake. The dots are the centroid locations of high-frequency energy release during the 2011 Tohoku-oki megathrust earthquake in time increments of 5 seconds with colour indicating time with respect to the hypocentral time (Kiser & Ishii 2012). Black contours show the area associated with the centroid locations of the Tohoku-oki earthquake and are calculated using the maximum value at each gridpoint from the normalized back-projection amplitudes at each centroid time. The 0.93 and 0.97 contours are plotted and the area above 0.97 is shown in light grey. The red star is the epicentre of the Tohoku-oki main shock (JMA catalogue). The parallel dashed lines and associated label (CG) show the along strike location of the Tohoku-oki coseismic gap from Kiser & Ishii (2013). The line with triangles is the location of the Japan trench. On- and off-shore regions are shown with white and dark grey background colours, respectively. The black dashed rectangle is the region shown in (b). The inset shows the regional context of the study area. (b) Dots are the centroid locations of high-frequency energy release during the 2021 M_w 7.1 Fukushima earthquake in time increments of 1 s with colour indicating time with respect to the hypocentral time. The white squares are the epicentres of aftershocks during the first 5 d following the Fukushima earthquake (JMA catalogue). White contours are the same as in (a). (c) The light grey and pink areas are the imaged rupture areas of the 2010 M_w 8.8 and 2012 M_w 7.1 Chile earthquakes, respectively, modified from (Kiser & Ishii 2013). The red and black stars are the epicentres of the 2010 M_w 8.8 and 2012 M_w 7.1 Chile earthquakes, respectively [National Earthquake Information Center (NEIC) catalogue]. The line with triangles is the location of the Peru-Chile trench. All other plotting details are the same as (a).

using the 1-D seismic velocity model IASP91 (Kennett & Engdahl 1991). Initial *P*-wave arrivals from one of the aftershocks (M_w 5.3, 15 February 2021 12:26:04 UTC) of the Fukushima main shock are time shifted to the hypocentre of the event and then aligned using an empirical cross-correlation approach (Ishii *et al.* 2007). This step corrects for the 3-D seismic velocity structure of the Earth, and the resulting traveltime corrections are added to the theoretical traveltimes for the back-projection analysis. A coherency-based back-projection method (Ishii 2011), which reduces smearing artefacts in the source images, is used to determine the centroid locations of imaged energy throughout the Fukushima earthquake. A separate linear back-projection analysis (Ishii *et al.* 2005) is performed to determine the relative amplitude of energy release throughout the rupture (Fig. S1). The amplitudes of all back-projection results are evaluated as a function of time using a 10-s averaging window.

Results from the back-projection analysis show a northeast/southwest bilateral rupture with a total length of approximately 56 km and duration of around 30 s (Fig. 1b; Movie S2). The initial 8 seconds of the rupture are dominated by southwest propagation at a speed of approximately 1.9 km s^{-1}. Following this, the rupture transitions to a northeast propagation direction at a speed of 2.5 km s^{-1}. A comparison between these results and the Tohoku-oki coseismic gap shows that the rupture area of the M_w 7.1 earthquake filled a significant portion of this gap (Fig. 1a). The imaged rupture area of the M_w 7.1 event is also significantly larger than the resolution kernel associated with the seismic array used in the back-projection analysis (Fig. S2), indicating that the inferred rupture area is controlled by the source properties of the event and not limitations in spatial resolution.

As with the 2012 M_w 7.1 earthquake that filled the 2010 Maule, Chile coseismic gap, the Fukushima event is the only major ($M_w \geq 7$) thrust faulting aftershock to occur within the Tohoku-oki megathrust rupture area. One potential difference associated with the Fukushima earthquake compared to the Maule, Chile earthquake sequence is that the reported depth of the Fukushima event is slightly below the inferred plate interface depth at this location (Hayes *et al.* 2018), and therefore this event may have actually occurred in the subducting Pacific Plate as opposed to the plate interface. Though this may indicate differences in the details of how the coseismic gaps were filled, in both the Tohoku, Japan and Maule, Chile cases these sections of the subduction zone were evidently primed for future large events by their respective main shock ruptures. In the case of the Tohoku-oki coseismic gap, slip from the 2011 megathrust earthquake surrounding this region would be expected to increase compressional stresses in this section of the subducting slab (e.g. Astiz *et al.* 1988). It is possible that thrust faulting within this compressed section of subducting slab accommodated the stress changes associated with the coseismic gap as opposed to failure on the plate interface. The Maule, Chile and Tohoku-oki, Japan megathrust earthquakes provide the best imaged cases of this coseismic gap phenomenon, however, there is evidence of other megathrust events exhibiting this same behaviour. For example, though the initial back-projection analysis of the 2004 M_w 9.1 Sumatra–Andaman earthquake focused on the event's general

rupture properties, it was noted that the rupture exhibited intermittent energy release around the Nicobar Islands (Ishii *et al.* 2005). As in the Chile and Japan cases, the only major thrust faulting aftershock (M_w 7.2 in 2004) within the general rupture area of the Sumatra-Andaman megathrust earthquake occurred within this discontinuous section of the rupture and thus could represent an area where a coseismic gap formed and was quickly filled by the 2004 M_w 7.2 aftershock.

Both of the Chile and Japan coseismic gaps occur near the downdip end of the seismic plate interface. This region is characterized by heterogeneous frictional properties, which would be expected to produce the irregular ruptures observed during megathrust earthquakes (Lay *et al.* 2012). The correspondence between coseismic gaps of the 2010 Maule, Chile and 2011 Tohoku-oki, Japan megathrust earthquakes and the rupture areas of their large aftershocks suggests that coseismic gaps can be used to predict the locations of future large aftershocks. Aftershock forecasting is typically performed using statistical models that incorporate empirical observations of seismicity (e.g. ETAS; Ogata 1988) and physical models that calculate stress changes in the surrounding crust due to slip on the rupture surface of a main shock (e.g. Coulomb stress change; King *et al.* 1994). These models are effective at estimating aftershock seismicity rates and magnitude distributions, as well as the regions where faults of certain orientations are more likely to fail following the main shock. The observations of this study show that when evaluating where large aftershocks are likely to occur within the rupture surfaces of main shocks, clear evidence of coseismic gaps warrants a more deterministic approach to evaluating seismic hazards that utilizes information about where faults have and have not failed in recent earthquakes (McCann *et al.* 1979). The downdip locations of the coseismic gaps imply that the aftershocks will produce high frequency seismic waves that can cause widespread strong ground shaking and significant damage, as observed during the 2021 Fukushima event. Therefore, identification of coseismic gaps through detailed rupture analyses such as back-projection and finite-fault modelling (Ide 2007; Kiser & Ishii 2017) is critical for seismic hazard mitigation.

ACKNOWLEDGEMENTS

The Generic Mapping Tools (GMT) were used to create figures presented in this manuscript (Wessel *et al.* 2019). We thank Miaki Ishii for helpful feedback on the initial draft of this paper

AUTHOR CONTRIBUTIONS

Eric Kiser conceptualized, wrote and made figures for the original draft of the paper. Eric Kiser and Haiyang Kehoe performed the back-projection analysis and edited the text of the paper.

COMPETING INTERESTS

Authors declare that they have no competing interests.

DATA AVAILABILITY

All seismic data were downloaded through the IRIS Wilber 3 system (https://ds.iris.edu/wilber3/) including the following seismic networks https://doi.org/10.7914/SN/AZ, https://doi.org/10.7932/BDSN, https://doi.org/10.7914/SN/CC, https://doi.org/10.7914/SN/CI, https://doi.org/10.7914/SN/GS, https://doi.org/10.7914/SN/II, https://doi.org/10.7914/SN/IU, https://doi.org/10.7914/SN/IW, https://doi.org/10.21766/SSNMX/SN/MX, https://doi.org/10.7914/SN/OO, https://doi.org/10.7914/SN/PY, https://doi.org/10.7914/SN/TX, https://doi.org/10.7914/SN/US, https://doi.org/10.7914/SN/UU and https://doi.org/10.7914/SN/UW.

REFERENCES

Asano, K., & Iwata, T., 2012. Source model for strong ground motion generation in the frequency range 0.1–10 Hz during the 2011 Tohoku earthquake, *Earth, Planets Space,* **64**(12), 1111–1123.

Astiz, L., Lay, T., & Kanamori, H., 1988. Large intermediate-depth earthquakes and the subduction process, *Phys. Earth planet. Inter.,* **53**(1-2), 80–166.

Corbi, F., Funiciello, F., Brizzi, S., Lallemand, S., & Rosenau, M., 2017. Control of asperities size and spacing on seismic behavior of subduction megathrusts, *Geophys. Res. Lett.,* **44**(16), 8227–8235.

Ekström, G., Nettles, M. & Dziewonski, A.M., 2012. The global CMT project 2004–2010: Centroid-moment tensors for 13,017 earthquakes, *Physics of the Earth and Planetary Interiors,* **200,** 1–9.

Hayes, G. P., Moore, G. L., Portner, D. E., Hearne, M., Flamme, H., Furtney, M. & Smoczyk, G. M., 2018. Slab2, a comprehensive subduction zone geometry model, *Science,* **362**(6410), 58–61.

Ide, S., 2007. Slip inversion, *Treat. Geophys.,* **4,** 193–224.

Ishii, M., 2011. High-frequency rupture properties of the M w 9.0 off the Pacific coast of Tohoku Earthquake, *Earth, Planets Space,* **63**(7), 609–614.

Ishii, M., Shearer, P. M., Houston, H., & Vidale, J. E., 2007. Teleseismic P wave imaging of the 26 December 2004 Sumatra-Andaman and 28 March 2005 Sumatra earthquake ruptures using the Hi-net array, *J. geophys. Res.,* **112**(B11),.

Ishii, M., Shearer, P. M., Houston, H. & Vidale, J. E., 2005. Extent, duration and speed of the 2004 Sumatra–Andaman earthquake imaged by the Hi-Net array, *Nature,* **435**(7044), 933.

Kaneko, Y., Avouac, J.-P., & Lapusta, N., 2010. Towards inferring earthquake patterns from geodetic observations of interseismic coupling, *Nat. Geosci.,* **3**(5), 363–369.

Kennett, B., & Engdahl, E., 1991. Traveltimes for global earthquake location and phase identification, *Geophys. J. Int.,* **105**(2), 429–465.

King, G. C., Stein, R. S., & Lin, J., 1994. Static stress changes and the triggering of earthquakes, *Bull. seism. Soc. Am.,* **84**(3), 935–953.

Kiser, E. & Ishii, M., 2012. The March 11, 2011 Tohoku-oki earthquake and cascading failure of the plate interface, *Geophys. Res. Lett.,* **39**(7).

Kiser, E., & Ishii, M., 2013. The 2010 Maule, Chile, coseismic gap and its relationship to the 25 March 2012 M w 7.1 earthquake, *Bull. seism. Soc. Am.,* **103**(2A), 1148–1153.

Kiser, E., & Ishii, M., 2017. Back-projection imaging of earthquakes, *Ann. Rev. Earth planet. Sci.,* **45,** 271–299.

Lay, T. *et al.*, 2012. Depth-varying rupture properties of subduction zone megathrust faults, *J. geophys. Res.,* **117**(B4),.

McCann, W., Nishenko, S., Sykes, L., & Krause, J., 1979. Seismic gaps and plate tectonics: seismic potential for major boundaries, in *Earthquake Prediction And Seismicity Patterns* , pp. 1082–1147, Springer.

Ogata, Y., 1988. Statistical models for earthquake occurrences and residual analysis for point processes, *J. Am. Stat. Assoc.,* **83**(401), 9–27.

Reasenberg, P. A. & Jones, L. M., 1989. Earthquake hazard after a mainshock in California, *Science,* **243**(4895), 1173–1176.

Stein, S. & Liu, M., 2009. Long aftershock sequences within continents and implications for earthquake hazard assessment, *Nature,* **462**(7269), 87–89.

Utsu, T., 1970. Aftershocks and earthquake statistics (1): some parameters which characterize an aftershock sequence and their interrelations, *J. Faculty Sci.,* **3**(3), 129–195.

Wang, D., & Mori, J., 2011. Rupture process of the 2011 off the Pacific coast of Tohoku Earthquake (M w 9.0) as imaged with back-projection of teleseismic P-waves, *Earth, Planets Space,* **63**(7), 603–607.

Wessel, P., Luis, J., Uieda, L., Scharroo, R., Wobbe, F., Smith, W., & Tian, D., 2019. The generic mapping tools version 6, *Geochem., Geophys., Geosyst.,* **20**(11), 5556–5564.

Wetzler, N., Lay, T., Brodsky, E. E., & Kanamori, H., 2018. Systematic deficiency of aftershocks in areas of high coseismic slip for large subduction zone earthquakes, *Sci. Adv.,* **4**(2), eaao3225.

Yao, H., Shearer, P. M., & Gerstoft, P., 2012. Subevent location and rupture imaging using iterative backprojection for the 2011 Tohoku M w 9.0 earthquake, *Geophys. J. Int.,* **190**(2), 1152–1168.

SUPPORTING INFORMATION

Supplementary data are available at *GJI* online.

Figure S1. (a) Distribution of seismic stations (blue triangles) used in the back-projection analysis of the 2021 M_w 7.1 Fukushima earthquake. (b) Relative source–time function of the 2021 M_w 7.1 Fukushima earthquake. Time is with respect to the hypocentre time.

Figure S2. White contours show normalized integrated stack amplitudes from the back-projection analysis of the 2021 M_w 7.1 Fukushima earthquake. Contours greater than or equal to 0.7 are plotted using an interval of 0.1. Red contours show normalized integrated stack amplitudes from the back-projection analysis of a M_w 5.3 aftershock that occurred on 15 February 2021. Contours greater than or equal to 0.7 are plotted using an interval of 0.1.

Movie S1. Movie of the 2011 M_w 9.1 Tohoku-oki earthquake high-frequency (0.8–2.0 Hz) back-projection results (Kiser & Ishii, 2012). Dark red to dark blue represents high amplitude to low amplitude back-projection stack amplitudes, respectively. The colour scale is normalized to the maximum amplitude as a function of time. The red star is the epicentre from the JMA catalogue. The yellow line is the Japan trench. The white line is the coast of Japan. UTC time is shown in the upper right corner.

Movie S2. Movie of the 2021 M_w 7.1 Fukushima back-projection results. White to blue represents high amplitude to low amplitude back-projection stack amplitudes, respectively. The black star is the epicentre from the JMA catalogue. The white line is the coast of Japan. Time with respect to the hypocentral time is shown in the upper left corner.

Please note: Oxford University Press is not responsible for the content or functionality of any supporting materials supplied by the authors. Any queries (other than missing material) should be directed to the corresponding author for the paper.